J. Fluid Mech. (2017), *vol.* 819, R1, doi:10.1017/jfm.2017.184

Solvo-osmotic flow in electrolytic mixtures

Sela Samin[1,†] **and René van Roij**[1]

[1]Institute for Theoretical Physics, Center for Extreme Matter and Emergent Phenomena, Utrecht University, Princetonplein 5, 3584 CC Utrecht, The Netherlands

(Received 14 January 2017; revised 21 March 2017; accepted 21 March 2017; first published online 18 April 2017)

We show that an electric field parallel to an electrically neutral surface can generate flow of electrolytic mixtures in small channels. We term this solvo-osmotic flow, since the flow is induced by the asymmetric preferential solvation of ions at the liquid–solid interface. The generated flow is comparable in magnitude to the ubiquitous electro-osmotic flow at charged surfaces, but for a fixed surface charge density, it differs qualitatively in its dependence on ionic strength. Solvo-osmotic flow can also be sensitively controlled with temperature. We derive a modified Helmholtz–Smoluchowski equation that accounts for these effects.

Key words: micro-/nano-fluid dynamics

1. Introduction

The use of electric fields to drive flow parallel to charged surfaces at the micro- and nano-scale is ubiquitous in science and technology, with applications in numerous fields, from 'Lab-on-a-Chip' devices (Stone, Stroock & Ajdari 2004; Squires & Quake 2005) and nano-fluidics (Bocquet & Charlaix 2010) to membrane and soil science, and the separation and analysis of biological macromolecules (Eijkel & Berg 2005). In its simplest form, the fluid velocity v_∞ far from the charged surface is proportional to the applied electric field E_0, $v_\infty = \mu_e E_0$. The electro-osmotic mobility μ_e is given by the Helmholtz–Smoluchowski equation (von Smoluchowski 1903), $\mu_e = -\varepsilon\zeta/\eta$, where ε is the solvent permittivity, η is the solvent viscosity, and the so-called zeta potential ζ is the electric potential at the shear plane. In neat (single-component) solvents, this electro-osmotic flow (EOF) has been studied extensively (Delgado *et al.* 2007), with more recent works focusing on the influence of the channel geometry (Bhattacharyya, Zheng & Conlisk 2005; Mao, Sherwood & Ghosal 2014), surface slip (Bouzigues, Tabeling & Bocquet 2008; Huang *et al.* 2008; Maduar *et al.* 2015; Rankin & Huang 2016), ion specificity (Huang *et al.* 2007) and solvent rheology (Bautista *et al.* 2013). Electro-osmotic flow in solvent mixtures is common in non-aqueous capillary electrophoresis (Kenndler 2014), and has been investigated also for aqueous mixtures (Valkó, Sirén & Riekkola 1999; Grob & Steiner 2002), but the electrokinetics in such systems is not well understood.

† Email address for correspondence: S.Samin@uu.nl

The difference between the electrostatics of neat solvents and solvent mixtures has also been an area of intense research in recent years, with the growing use of miscible and non-miscible oil–water mixtures in colloidal science and microfluidics. A crucial role is played by the partitioning of ions between solvents, due to their preferential solvation in one of the liquids (Onuki & Kitamura 2004; Tsori & Leibler 2007; Zwanikken & van Roij 2007; Araki & Onuki 2009; Ben-Yaakov *et al.* 2009; Bier *et al.* 2011; Okamoto & Onuki 2011; Pousaneh & Ciach 2011; Samin & Tsori 2011, 2013; Bier, Gambassi & Dietrich 2012; Samin & Tsori 2012; Pousaneh & Ciach 2014; Michler *et al.* 2015; Samin & Tsori 2016). The preferential wetting of one liquid at a solid surface or the presence of a liquid–liquid interface therefore also affects the electrostatics of the mixture. It leads to a modification of colloid–colloid (Law, Petit & Beysens 1998; Hertlein *et al.* 2008; Bonn *et al.* 2009; Nellen *et al.* 2011; Samin *et al.* 2014) as well as colloid–interface interactions (Leunissen *et al.* 2007*a*,*b*; Banerjee *et al.* 2016; Elbers *et al.* 2016; Everts, Samin & van Roij 2016). The strength of preferential solvation is measured by the Gibbs transfer energy k_BTg^α of an ion species α between two solvents, where k_BT is the thermal energy and $|g^\alpha| \sim 1$–10 for aqueous mixtures of relatively polar organic solvents (Kalidas, Hefter & Marcus 2000; Marcus 2007), but can be as large as 15 in less polar solvents containing antagonistic salts (Onuki *et al.* 2016). For monovalent salts dissolved in mixtures, the combined effect of both ionic species (Bier *et al.* 2011; Okamoto & Onuki 2011; Samin & Tsori 2013; Michler *et al.* 2015) is conveniently expressed in terms of the average overall solubility $g_S = (g^+ + g^-)/2$ and the solubility contrast $g_D = (g^+ - g^-)/2$, which, for example, determines the Donnan potential k_BTg_D/e at oil–water interfaces due to ion partitioning, where e is the elementary charge. In this work, we show that preferential solvation also affects electrokinetic phenomena in mixtures, where it generates an additional, and significant, source of fluid mobility. We find that the dominant contribution to this additional mobility is proportional to g_D and independent of the surface charge, and is therefore able to generate flow even at electrically neutral surfaces.

2. Formulation of the problem

Within a continuum theory, we study the flow in a channel containing an electrolytic mixture using direct numerical simulations and a simple linear theory. We consider an oil–water mixture characterized by the order parameter φ, which is the deviation of the volume fraction of water in the mixture, ϕ, from its critical value ϕ_c: $\varphi = \phi - \phi_c$. The mixture contains point-like monovalent ions with number densities $n^\pm$. In our calculations, two cylindrical reservoirs containing the mixture are coaxially connected by a long cylindrical channel with radius R, with the z axis being the axis of symmetry and r the radial coordinate. In equilibrium, the composition in both of the reservoirs is $\varphi_0 = 0$ and the number densities of ions are n_0. At the edge of one reservoir, we impose a uniform external electric field $E_0\hat{z}$, forcing the charged mixture in the channel, and leading to a flow field $\boldsymbol{v}$.

2.1. *Governing equations*

To study the mixture dynamics, we start from a free energy F of the form

$$\beta F = \int \mathrm{d}\boldsymbol{r}\left\{f_m(\varphi) + \frac{C}{2}|\nabla\varphi|^2 + \frac{\beta}{2}\varepsilon(\varphi)(\nabla\psi)^2 + \sum_{\alpha=\pm} n^\alpha[(\log(v_0 n^\alpha) - 1) - g^\alpha\varphi]\right\}, \tag{2.1}$$

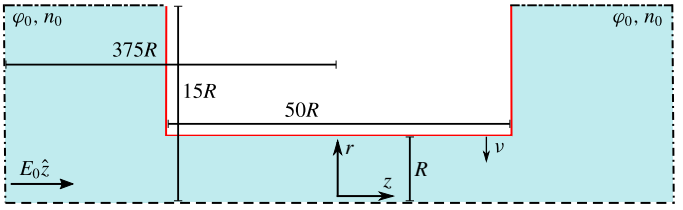

FIGURE 1. An illustration of the system in the rOz plane. A cylindrical channel with radius R connects two reservoirs containing a salty water–acetonitrile mixture with a composition $\varphi_0 = 0$ and a salt concentration n_0. The system is driven out of equilibrium by an external electric field E_0 in the $\hat{z}$ direction. The system dimensions, given in the figure in terms of R, ensure that the effect of reservoirs and channel edges on the flow that develops in the channel is small. Different boundary line types indicate different boundary conditions (see text).

where $\beta^{-1} = k_B T$ and $v_0 = a^3$ is the molecular volume of both mixture components. The first term in the integrand is the 'double-well' bulk mixture free energy density, $v_0 f_m = (\chi - 2)\varphi^2 + 4\varphi^4/3$, where $\chi \sim 1/T$ is the Flory parameter. This free energy leads to an upper critical solution temperature type phase diagram, with a critical temperature T_c and the corresponding critical Flory parameter $\chi_c = 2$. In this work, we focus on the region $T > T_c$ ($\chi < \chi_c$), such that the bulk mixture is always homogeneous. The second 'square gradient' term accounts for composition inhomogeneities at interfaces, where $C = \chi/a$. The third term is the electrostatic energy density, where ψ is the electric potential and $\varepsilon(\varphi)$ is the permittivity, assumed to depend linearly on φ. The final term in the integrand is the ionic free energy, composed of the ideal-gas entropy of ions of species $\alpha = \pm$ and the ionic solvation energy, which is proportional to the Gibbs free energy of transfer g^α and local solvent composition. It should be noted that g^α can vary greatly between ionic species depending on their size, charge and chemistry.

The relations governing the mixture dynamics read (Araki & Onuki 2009)

$$\partial\varphi/\partial t + \boldsymbol{\nabla}\cdot(\varphi\boldsymbol{v}) = D^m\nabla^2\beta\mu, \tag{2.2}$$

$$\partial n^\alpha/\partial t + \boldsymbol{\nabla}\cdot(n^\alpha\boldsymbol{v}) = D^\alpha\boldsymbol{\nabla}\cdot n^\alpha\boldsymbol{\nabla}\beta\lambda^\alpha, \tag{2.3}$$

$$\boldsymbol{\nabla}\cdot(\varepsilon(\varphi)\boldsymbol{\nabla}\psi) = -\sum_\alpha z^\alpha n^\alpha, \tag{2.4}$$

$$\boldsymbol{\nabla}\cdot\boldsymbol{v} = 0, \tag{2.5}$$

$$\eta\nabla^2\boldsymbol{v} - \boldsymbol{\nabla}p = v_0^{-1}\varphi\boldsymbol{\nabla}\mu + \sum_\alpha n^\alpha\boldsymbol{\nabla}\lambda^\alpha. \tag{2.6}$$

Equation (2.2) is the convective Cahn–Hilliard equation, where D^m is the interdiffusion constant of the mixture and $\mu = v_0(\delta F/\delta\varphi)$ is the solvent chemical potential, given by $\beta\mu/v_0 = -C\nabla^2\varphi + f'(\varphi) - \beta\varepsilon'(\varphi)(\boldsymbol{\nabla}\psi)^2/2 - \sum_\alpha g^\alpha n^\alpha$. Equations (2.3) and (2.4) are the Poisson–Nernst–Planck equations, where the D^α are ionic diffusion constants and $\lambda^\alpha = \delta F/\delta n^\alpha$ are the ionic chemical potentials given by $\beta\lambda^\alpha = \log(v_0 n^\alpha) + \beta z^\alpha\psi - g^\alpha\varphi$, with $z^\alpha = \pm e$. Equations (2.5) and (2.6) are the Stokes equations at small Reynolds number, where p is the pressure and the right-hand side of (2.6) contains the body forces due to concentration gradients.

An illustration of the computational domain for the numerical solution of (2.2)–(2.6) is shown in figure 1 (not to scale). Solid walls are indicated by the red lines in

figure 1. On these walls, we impose the no-slip boundary condition (BC) for the velocity, $\boldsymbol{v} = 0$, and no material fluxes for the composition and ions. The second BC for the composition is $-\boldsymbol{\nu} \cdot \nabla\varphi = \gamma$, with $\boldsymbol{\nu}$ being the unit normal to the surface. The coefficient γ represents the short-range interaction between the solvent mixture and the surface (per solvent molecule). We call γ the effective surface field; γ is positive (negative) for hydrophilic (hydrophobic) surfaces. The surface may carry a fixed charge density $e\sigma$, which from Gauss's law implies $-\boldsymbol{\nu} \cdot \nabla\psi = e\sigma/\varepsilon(\varphi)$.

At the open reservoir edges, indicated by dash–dot lines in figure 1, we set the composition to $\varphi_0 = 0$ and the ion densities to n_0. We also allow the mixture to be freely advected, with vanishing total stress and diffusive fluxes, $-\boldsymbol{\nu} \cdot (p\boldsymbol{1} + \boldsymbol{S} - \boldsymbol{T}) = 0$, $-\boldsymbol{\nu} \cdot \nabla\mu = 0$ and $-\boldsymbol{\nu} \cdot n^{\pm}\nabla\lambda^{\pm} = 0$ respectively, where $\boldsymbol{T} = \eta(\nabla\boldsymbol{v} + \nabla\boldsymbol{v}^{\mathrm{T}})$ is the viscous stress tensor and $\boldsymbol{S}$ is the total stress tensor, given by

$$\beta\boldsymbol{S} = \left[\varphi f_m'(\varphi) - f_m - \frac{C}{2}|\nabla\varphi|^2 - C\varphi\nabla^2\varphi - \varphi\varepsilon'(\varphi)\frac{|\boldsymbol{E}|^2}{2} + \frac{\boldsymbol{E}\cdot\boldsymbol{D}}{2} + \sum_{\alpha=\pm}(1 - g^{\alpha}\varphi)n^{\alpha}\right]\boldsymbol{1} + C\nabla\varphi\nabla\varphi - \boldsymbol{E}\boldsymbol{D}, \tag{2.7}$$

where $\boldsymbol{E} = -\nabla\psi$ is the electric field, $\boldsymbol{D} = \varepsilon(\varphi)\boldsymbol{E}$ is the displacement field and the prime indicts differentiation with respect to the argument. Lastly, the dashed curve in figure 1 is the $r = 0$ axis, where we apply symmetry BCs for all fields. The numerical simulations in this work were performed using the finite-elements software COMSOL multiphysics.

2.2. *Linear theory*

To better understand the flow generated in the channel, we first consider a simplified system where we assume that (i) perturbations in the composition $\varphi - \varphi_0$ and ion densities $\delta n^{\pm} = n^{\pm} - n_0$ relative to their bulk values are small due to weak adsorption at the channel surface, (ii) the channel is very long such that edge effects are negligible and translational invariance in the z direction applies, (iii) the dominant body force in (2.6) is the electric body force and (iv) convective composition and ion currents in the channel are negligible since the corresponding Péclet numbers are small. However, even in simple mixtures, transport through channels can lead to complex and surprising effects (Samin & van Roij 2017), also for small Péclet numbers. Therefore, it is necessary to also solve the complete system equations (2.2)–(2.6) numerically to verify that the simplified description is valid.

Within the appropriate parameter regime, the full transport problem can thus be reduced to a steady-state problem, where all fields depend only on r. We also decompose the electric potential as $\psi(r, z) = \Psi(r)/(\beta e) - zE_z + \text{const.}$, where $\Psi(r)$ is a dimensionless radial potential and E_z is the uniform axial electric field in the channel. It should be noted that $E_z \neq E_0$ in general. For a fully developed flow, we assume that $v_r = 0$ and thus $v_z = v_z(r)$ from (2.5). Lastly, we set $\nabla p = 0$ as we focus on the effect of E_z. Linearizing the simplified equations (2.2)–(2.6) (Okamoto & Onuki 2011; Samin & Tsori 2013), we find $\delta n^{\pm} = n_0(g^{\pm}\varphi \mp \Psi)$ and obtain the system

$$\xi^2\nabla_r^2\varphi = \varphi + 2n_0 g_D(\Psi - g_D\varphi)/\tau, \tag{2.8}$$

$$\lambda_D^2\nabla_r^2\Psi = \Psi - g_D\varphi, \tag{2.9}$$

$$\lambda_D^2\eta\nabla_r^2 v_z = \bar{\varepsilon}(\Psi - g_D\varphi)E_z/(\beta e), \tag{2.10}$$

where $\xi = (C/\tau)^{1/2}$ is the modified correlation length and $\tau = 2(2-\chi)/v_0 - 2n_0 g_S^2$. The Debye length is $\lambda_D = (8\pi l_B n_0)^{-1/2}$, where $l_B = e^2/(4\pi\bar{\varepsilon}k_B T)$ is the Bjerrum length with the average permittivity $\bar{\varepsilon} = \varepsilon(\varphi_0)$.

3. Results

In a cylindrical domain, the profiles $\varphi(r)$ and $\Psi(r)$ of (2.8) and (2.9) are the linear combinations

$$\Psi(r) = a_1 \mathrm{I}_0(q_1 r) - a_2 \mathrm{I}_0(q_2 r), \tag{3.1}$$

$$\varphi(r) = b_1 \mathrm{I}_0(q_1 r) - b_2 \mathrm{I}_0(q_2 r), \tag{3.2}$$

where I_n is the modified Bessel function of the first kind of order n, such that the wavenumbers q_i $(i = 1, 2)$ obey the biquadratic equation

$$\lambda_D^2 q_i^4 - [1 + (\lambda_D/\xi)^2 - g_D^2/(4\pi l_B C)]q_i^2 + \xi^{-2} = 0. \tag{3.3}$$

The amplitudes a_i and b_i follow from symmetry at $r = 0$ and the BCs given above at the channel surface $r = R$. Also making use of the identity $((q_1\lambda_D)^2 - 1)((q_2\lambda_D)^2 - 1) = g_D^2/(4\pi l_B C)$, which follows from (3.3), the amplitudes read

$$a_i = \frac{g_D}{1 - (\lambda_D q_i)^2} b_i, \tag{3.4}$$

$$b_i = \frac{\gamma[1 - (\lambda_D q_i)^2] - g_D\sigma/C}{\lambda_D^2 q_i (q_2^2 - q_1^2)\mathrm{I}_1(q_i R)}. \tag{3.5}$$

We plot in figure 2(*a*) the resulting composition and potential profiles for a water–acetonitrile mixture with $n_0 = 50$ mM of NaCl ($\lambda_D = 1.16$ nm, $g^+ \approx 0$ and $g^- \approx 4$ (Kalidas *et al.* 2000; Marcus 2007)) at room temperature ($\chi = 1.86$, $\xi = 1.31$ nm) inside a channel with radius $R = 20\lambda_D$. The mixture physical properties are given in the caption of figure 2. We assume that these properties are independent of temperature, except for the mixture interdiffusion constant D^m, which follows from $D^m = (6\beta\pi\eta\xi)^{-1}$ (Kawasaki 1970). The ionic diffusion constants are taken to be $D^\pm = 1 \times 10^{-9}$ m^2 s^{-1}.

The channel surface is uncharged ($\sigma = 0$), but is hydrophilic ($\gamma = 0.2C > 0$), resulting in the adsorption of water near the wall. Since the anions are hydrophilic, the water 'drags' them along, and hence the anions also effectively adsorb at the surface; see the ionic profiles in figure 2(*b*). Although the cations are indifferent to the local composition, they also adsorb at the surface due to electrostatics, but are distributed more broadly. The result is an electric double layer at an uncharged surface (Samin & Tsori 2013; Samin *et al.* 2014), even though this layer is overall charge neutral. Figure 2 shows good agreement between the full numerical solutions and the linear theory. The numerical profiles of φ and $n^\pm$ decay to values that slightly differ from their bulk values due to a weak nonlinear effect induced by solvation (Samin & Tsori 2016). The thickness of the charged layer at the surface, $\rho(r) = 2en_0(g_D\varphi - \Psi)$, could be estimated in experiments from the characteristic lengths q_i^{-1}. These length scales are to be estimated from (3.3) given data for λ_D, ξ and g_D.

Although the fluid is overall neutral, the negative ion layer is more strongly adsorbed at the wall. When an external axial electric field is applied, this layer then serves as an effective surface charge, and the adjacent positively charged layer as an

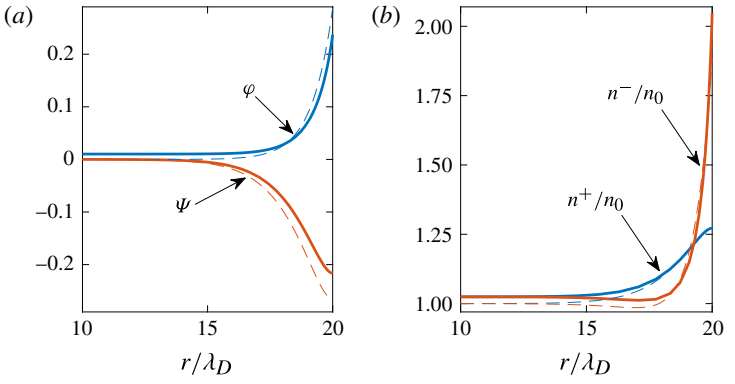

FIGURE 2. (*a*) Composition $\varphi(r)$ and scaled potential $\Psi(r)$ at the channel centre ($z=0$) and (*b*) the corresponding scaled cation and anion profiles, for a water–acetonitrile mixture with a Debye length $\lambda_D = 1.16$ nm and a correlation length $\xi = 1.31$ nm. The solid lines represent the numerical solution and the dashed curves represent the linear theory (see text). We plot the profiles near the channel surface, where here and in all other figures the channel radius is $R = 20\lambda_D$. The channel surface is uncharged ($\sigma = 0$) and hydrophilic, $\gamma = 0.2C$, corresponding to a tension of ≈ 7 mN m^{-1}. The mixture with $\bar{\varepsilon} = 58$ and at a temperature of 293 K ($\chi = 1.86$) contains 50 mM of NaCl ($g^+ = 0$, $g^- = 4$). For the mixture properties, we use the critical temperature $T_c = 272$ K and a molecular length $a = 3.6$ Å, estimated from a critical density of 900 kg m^{-3} and a viscosity of 0.7 mPa s (Sazonov *et al.* 2007; Wohlfarth 2009). The liquid permeability is given by $\varepsilon(\varphi)/\varepsilon_0 = \varepsilon_{acetonitrile}/2 + \varepsilon_{water}/2 + (\varepsilon_{water} - \varepsilon_{acetonitrile})\varphi$, where ε_0 is the vacuum permittivity, and we used $\varepsilon_{acetonitrile} = 36.6$ and $\varepsilon_{water} = 79.5$.

effective electric double layer. The result is an induced fluid flow, similar to EOF. The steady-state axial flow profile $v_z(r)$ is obtained by putting (3.1) and (3.2) into (2.10), and imposing the no-slip BC at $r = R$ and symmetry at $r = 0$,

$$v_z(r) = \frac{\bar{\varepsilon} E_z}{\beta e \eta} \sum_{i=1,2} (g_D b_i - a_i) \frac{\mathrm{I}_0(q_i r) - \mathrm{I}_0(q_i R)}{(-1)^i (\lambda_D q_i)^2}, \tag{3.6}$$

which for the parameters of figure 2 is plotted in figure 3 (labelled with $\sigma = 0$), showing reasonable agreement between the numerical solution and (3.6). Indeed, a flow is generated by the overall neutral but locally charged layer of fluid near the wall. Figure 3 shows that $v_z(r)$ quickly saturates to a plug-like flow of a few mm s^{-1}. We term this solvation-induced phenomenon solvo-osmotic flow (SOF). This flow is similar and comparable in magnitude to simple EOF, shown in figure 3 by the curve for a neat solvent with the same properties as the mixture, but near a weakly charged surface with $\sigma = -0.012$ nm^{-2}.

Solvo-osmotic flow can either combine with or work against EOF, as shown by two curves in figure 3, where we used the parameter of figure 2, but with non-zero surface charges, $\sigma = \pm 0.012$ nm^{-2}. For $\sigma < 0$, the result is an enhanced flow with the velocity at the channel centre slightly smaller than the sum of SOF and EOF on their own. In a neat solvent, when σ changes sign, one expects a simple change of sign also for the velocity. However, here SOF opposes EOF for $\sigma > 0$ and, for the parameters of figure 3, the result is that inside most of the channel v_z remains positive, but with a much smaller magnitude. There is, however, a weak backflow close to the channel

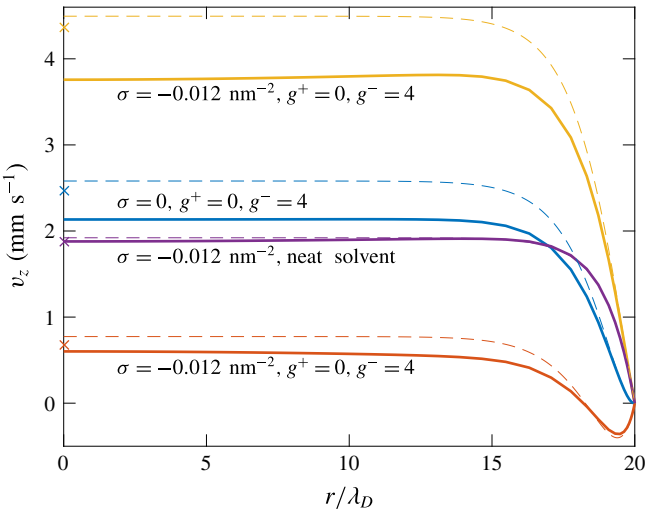

FIGURE 3. Axial velocity profiles $v_z(r)$ at an applied field of $E_0 = 2.5$ V mm^{-1} for several scenarios; see the labels on the figure. All other parameters are the same as in figure 2. The numerical results (solid curves) are in good agreement with the linear theory (dashed curves), where in (3.6) we used E_z from the numerical calculation. Crosses were calculated using (3.8).

wall resulting from the radial component of the body force in the fluid becoming significant in this case.

In the large-R limit where $R \gg \lambda_D, \xi$, the fluid moves as a plug, $v_z = \text{const.}$, and one defines the electro-osmotic mobility of the fluid as $\mu_e = v_z/E_z$. In this limit, we find

$$\mu_e = -\frac{\bar{\varepsilon}}{\eta}\frac{4\pi l_B \sigma (q_1^2 + q_2^2 + q_1 q_2 - \lambda_D^{-2}) + g_D \gamma \lambda_D^{-2}}{q_1 q_2 (q_1 + q_2)\beta e}. \tag{3.7}$$

Noting that the biquadratic equation (3.3) implies $q_1 q_2 = (\xi \lambda_D)^{-1}$ and $q_1^2 + q_2^2 = \xi^{-2} + \lambda_D^{-2}[1 - g_D^2/(4\pi l_B C)]$, and assuming that also $\lambda_D/\xi \gg |g_D|/(4\pi l_B C)$, equation (3.7) reduces to the modified Helmholtz–Smoluchowski equation

$$\mu_e = -\frac{\bar{\varepsilon}}{\eta}\left[\left(4\pi l_B \lambda_D \sigma + \frac{g_D \gamma \xi}{1 + \lambda_D/\xi}\right)\frac{1}{\beta e}\right]. \tag{3.8}$$

Equation (3.8) is the main result of this paper, where the term in brackets is the zeta potential ζ, with the shear plane located at $r = R$. Only the first term $\propto\sigma$ in (3.8) exists for a neat solvent (Keh & Tseng 2001). In a mixture, ζ is determined also by the properties of the salt and surface through the second term $\propto g_D\gamma$ in (3.8), which plays the role of an effective surface charge. The attractive feature of (3.8) is the ability to easily tune the fluid mobility through g_D without making any surface modification. For example, by replacing the anion Cl^- with the hydrophobic anion BPh_4^-, we have $g_D \approx 6$ (Marcus 2007) (instead of $g_D = -2$), which would then change μ_e drastically, in some cases even its sign. As we show below, the dependence of μ_e on ξ in mixtures opens the possibility to tune the mobility also with temperature, since ξ diverges near the mixture critical temperature. Nevertheless, we stress that $\xi \sim a$ for

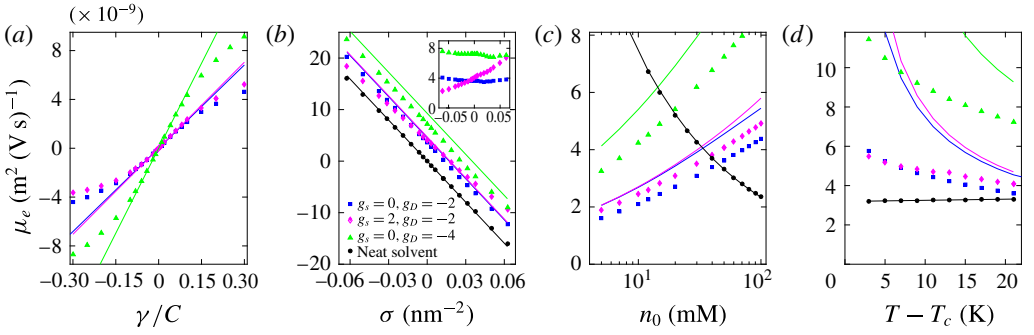

FIGURE 4. Dependence of the fluid mobility μ_e on (*a*) the surface–solvent coupling γ, (*b*) the surface charge $e\sigma$, (*c*) the salt concentration n_0 and (*d*) the temperature T, for three types of electrolytic mixture (see text). Symbols correspond to numerical results and lines to (3.8). In (*b–d*), we plot also μ_e for a neat solvent with the same physical properties as the mixtures (circles). In (*a–c*), $T = 293$ K is fixed, while in (*a*,*b*,*d*) we keep $n_0 = 50$ mM fixed. For the mixture data sets in (*b–d*), we took $\gamma = 0.2C$, and in (*a*,*c*,*d*), we took $\sigma = 0$. For the neat solvent in (*c*,*d*), we used $\sigma = 0.012$ nm^{-2}. The inset of (*b*) shows the shift in mobility between the mixtures and the neat solvent.

completely miscible mixtures (the $\chi \to 0$ limit in our theory). Hence, equation (3.8) should be applicable to mixtures in general, and, as the crosses in figure 3 confirm, it is in good agreement with the numerical results for $v_z(0)$.

In figure 4, we show the effects of varying some of the free parameters of our model on the fluid mobility, and compare numerical results (symbols) with (3.8) (lines). We compare three types of electrolytic mixture, one containing NaCl (diamonds) as before and two containing so-called antagonistic salts in which one of the ions is hydrophilic and the other hydrophobic. In order to single out the role of g_D, we choose $g_S = 0$ by setting $g^- = -g^+ = 2$ (squares) and 4 (triangles). Figure 4(*a*) shows the pure SOF mobility as a function of the surface field γ, revealing that the linear theory becomes an excellent approximation for small enough $|\gamma|$, for which $\varphi \ll 1$ holds, and that μ_e increases with γ and g_D, as expected from (3.8). It should be noticed that the sign of μ_e depends on the wetting properties of the surface. For the salts having the same solubility contrast g_D but different overall solubility g_S (squares and diamonds), we find significant differences in the mobility only for large enough $|\gamma|$. In this regime, the entropy decrease of the ions near the wall hinders their adsorption, leading to a reduced mobility compared with the linear theory.

In figure 4(*b–d*), we also contrast the electrolytic mixtures with a neat solvent (circles) having the same physical properties as the mixtures. In figure 4(*b*), we examine the effect of adding a fixed surface charge σ. Clearly, here SOF increases the mobility compared with regular EOF in a neat solvent. The inset of figure 4(*b*) shows that the shift in mobility is almost constant and increases with g_D for the antagonistic salts, as expected from (3.8). The mobility shift is not constant for NaCl, rather it increases with σ, and the result is an asymmetry in the mobility when σ changes sign, an effect that is absent in neat solvents. This effect originates from the nonlinear coupling between electrostatics and solvation (Samin & Tsori 2012), and is expressed by the next-order term $\propto g_S \varphi \Psi$ in the expansion of $\delta n^{\pm}$. This contribution vanishes for our ideal antagonistic salts, but should be relevant for the majority of realistic salts. The relative shift in mobility due to SOF is significant for the weakly

to moderately charged surfaces we considered here, which is a common situation for hydrophobic surfaces (Jing & Bhushan 2013), or in hydrophilic surfaces near their iso-electric point. For typically highly charged hydrophilic surfaces, the contribution of SOF may be small, although this may not always be the case since both g_D and γ can be much larger than the values used in this work.

In figure 4(*c*,*d*), we show the influence of the salt concentration and temperature respectively on mobility. In both panels, we compare electrolytic mixtures in an uncharged channel with a neat solvent in a channel with $\sigma = 0.012$ nm^{-2}. Strikingly, figure 4(*c*) shows that the mobility increases with n_0 for the mixtures, while it decreases for the neat solvent. This behaviour follows from the dependence of μ_e on $\lambda_D \propto n_0^{-1/2}$ in (3.8). For constant σ, the contribution to the surface potential from the first term in (3.8) becomes smaller when λ_D decreases, while the second term becomes larger. Figure 4(*c*) suggests that for $n_0 \sim 100$ mM, the contribution to the mobility from solvation could be dominant when the surface is weakly charged. The SOF is enhanced by increasing the ionic strength since this leads also to increased ion adsorption at the wall, which results in a larger effective surface charge. The opposite dependence on n_0 between the two terms in (3.8) can therefore lead to a minimum in the mobility of mixtures at charged surfaces, which is confirmed by numerical calculations (not shown).

Figure 4(*d*) demonstrates that, in mixtures, temperature can be used to effectively tune the mobility, whereas its effect is much smaller in neat solvents. The reason is that the correlation length ξ diverges as T_c is approached from the one-phase region at the critical composition. In (3.8), the mobility increases with ξ, or equivalently when the temperature is lowered towards T_c, which is confirmed by the numerical results in figure 4(*d*). Here, the agreement with the linear theory is not as good since φ is no longer small when T_c is approached. The numerical results show that μ_e changes by as much at 60 % in a temperature window of 20 K, whereas it essentially remains constant for the neat solvent. We did not account, however, for the change of ε with temperature. This effect will be at play for both mixtures and neat solvents, and should be smaller since, for example, the permittivity of water changes only by approximately 10 % in the same temperature window.

4. Conclusions

In conclusion, we have shown that the electro-osmotic mobility of mixtures contains an additional contribution due to the preferential solvation of ions. This contribution allows flow to be driven at an electrically neutral surface and the mobility to be varied significantly by changing the type of salt or the temperature. All of our results can be directly extended to the phoretic motion of particles in an applied field.

A comparison of our results with existing experiments (Valkó *et al.* 1999; Grob & Steiner 2002) is difficult to perform at this point, because capillary electrophoresis experiments employ fused silica surfaces, which are typically highly charged and, more importantly, charge-regulating. A modification of the theory is thus required to better mimic experimental conditions. This should include the chemical dissociation equilibrium at the channel surface, and the change in the fluid viscosity with composition. For the study of transient SOF, one should also consider the asymmetry in the cation and anion diffusion constants, and their dependence on the solvent composition. Our work points towards promising possibilities for the utilization of SOF in the transport of fluids through channels and of colloids by external fields, and we hope that it will lead to systematic experiments on the electrokinetics of solvent mixtures.

Acknowledgements

We acknowledge stimulating discussions with H. B. Eral. We thank the anonymous referees for their useful comments and suggestions. R.v.R. acknowledges financial support of a Netherlands Organisation for Scientific Research (NWO) VICI grant funded by the Dutch Ministry of Education, Culture and Science (OCW). S.S. acknowledges funding from the European Union's Horizon 2020 programme under the Marie Skłodowska-Curie grant agreement no. 656327. This work is part of the D-ITP consortium, a programme of the NWO funded by the OCW.

References

ARAKI, T. & ONUKI, A. 2009 Dynamics of binary mixtures with ions: dynamic structure factor and mesophase formation. *J. Phys.: Condens. Matter* **21** (42), 424116.

BANERJEE, A., WILLIAMS, I., AZEVEDO, R. N., HELGESON, M. E. & SQUIRES, T. M. 2016 Soluto-inertial phenomena: designing long-range, long-lasting, surface-specific interactions in suspensions. *Proc. Natl Acad. Sci. USA* **113** (31), 8612–8617.

BAUTISTA, O., SÁNCHEZ, S., ARCOS, J. C. & MÉNDEZ, F. 2013 Lubrication theory for electro-osmotic flow in a slit microchannel with the Phan-Thien and Tanner model. *J. Fluid Mech.* **722**, 496–532.

BEN-YAAKOV, D., ANDELMAN, D., HARRIES, D. & PODGORNIK, R. 2009 Beyond standard Poisson–Boltzmann theory: ion-specific interactions in aqueous solutions. *J. Phys.: Condens. Matter* **21** (42), 424106.

BHATTACHARYYA, S., ZHENG, Z. & CONLISK, A. T. 2005 Electro-osmotic flow in two-dimensional charged micro- and nanochannels. *J. Fluid Mech.* **540**, 247–267.

BIER, M., GAMBASSI, A. & DIETRICH, S. 2012 Local theory for ions in binary liquid mixtures. *J. Chem. Phys.* **137** (3), 034504.

BIER, M., GAMBASSI, A., OETTEL, M. & DIETRICH, S. 2011 Electrostatic interactions in critical solvents. *Europhys. Lett.* **95** (6), 60001.

BOCQUET, L. & CHARLAIX, E. 2010 Nanofluidics, from bulk to interfaces. *Chem. Soc. Rev.* **39**, 1073–1095.

BONN, D., OTWINOWSKI, J., SACANNA, S., GUO, H., WEGDAM, G. & SCHALL, P. 2009 Direct observation of colloidal aggregation by critical Casimir forces. *Phys. Rev. Lett.* **103** (15), 156101.

BOUZIGUES, C. I., TABELING, P. & BOCQUET, L. 2008 Nanofluidics in the Debye layer at hydrophilic and hydrophobic surfaces. *Phys. Rev. Lett.* **101**, 114503.

DELGADO, A. V., GONZÁLEZ-CABALLERO, F., HUNTER, R. J., KOOPAL, L. K. & LYKLEMA, J. 2007 Measurement and interpretation of electrokinetic phenomena. *J. Colloid Interface Sci.* **309** (2), 194–224.

EIJKEL, J. C. T. & VAN DEN BERG, A. 2005 Nanofluidics: what is it and what can we expect from it? *Microfluid Nanofluid* **1** (3), 249–267.

ELBERS, N. A., VAN DER HOEVEN, J. E. S., DE WINTER, D. A. M., SCHNEIJDENBERG, C. T. W. M., VAN DER LINDEN, M. N., FILION, L. & VAN BLAADEREN, A. 2016 Repulsive van der Waals forces enable Pickering emulsions with non-touching colloids. *Soft Matt.* **12** (35), 7265–7272.

EVERTS, J. C., SAMIN, S. & VAN ROIJ, R. 2016 Tuning colloid–interface interactions by salt partitioning. *Phys. Rev. Lett.* **117** (9), 098002.

GROB, M. & STEINER, F. 2002 Characteristics of the electroosmotic flow of electrolyte systems for nonaqueous capillary electrophoresis. *Electrophoresis* **23** (12), 1853.

HERTLEIN, C., HELDEN, L., GAMBASSI, A., DIETRICH, S. & BECHINGER, C. 2008 Direct measurement of critical Casimir forces. *Nature* **451** (7175), 172–175.

HUANG, D. M., COTTIN-BIZONNE, C., YBERT, C. & BOCQUET, L. 2007 Ion-specific anomalous electrokinetic effects in hydrophobic nanochannels. *Phys. Rev. Lett.* **98**, 177801.

HUANG, D. M., COTTIN-BIZONNE, C., YBERT, C. & BOCQUET, L. 2008 Massive amplification of surface-induced transport at superhydrophobic surfaces. *Phys. Rev. Lett.* **101** (6), 064503.

JING, D. & BHUSHAN, B. 2013 Quantification of surface charge density and its effect on boundary slip. *Langmuir* **29** (23), 6953–6963.

KALIDAS, C., HEFTER, G. & MARCUS, Y. 2000 Gibbs energies of transfer of cations from water to mixed aqueous organic solvents. *Chem. Rev.* **100** (3), 819–852.

KAWASAKI, K. 1970 Kinetic equations and time correlation functions of critical fluctuations. *Ann. Phys.* **61** (1), 1–56.

KEH, H. J. & TSENG, H. C. 2001 Transient electrokinetic flow in fine capillaries. *J. Colloid Interface Sci.* **242** (2), 450–459.

KENNDLER, E. 2014 A critical overview of non-aqueous capillary electrophoresis. Part I: mobility and separation selectivity. *J. Chromatogr.* A **1335**, 16–30.

LAW, B. M., PETIT, J.-M. & BEYSENS, D. 1998 Adsorption-induced reversible colloidal aggregation. *Phys. Rev.* E **57** (5), 5782–5794.

LEUNISSEN, M. E., VAN BLAADEREN, A., HOLLINGSWORTH, A. D., SULLIVAN, M. T. & CHAIKIN, P. M. 2007*a* Electrostatics at the oil–water interface, stability, and order in emulsions and colloids. *Proc. Natl Acad. Sci. USA* **104** (8), 2585–2590.

LEUNISSEN, M. E., ZWANIKKEN, J., VAN ROIJ, R., CHAIKIN, P. M. & VAN BLAADEREN, A. 2007*b* Ion partitioning at the oil–water interface as a source of tunable electrostatic effects in emulsions with colloids. *Phys. Chem. Chem. Phys.* **9**, 6405–6414.

MADUAR, S. R., BELYAEV, A. V., LOBASKIN, V. & VINOGRADOVA, O. I. 2015 Electrohydrodynamics near hydrophobic surfaces. *Phys. Rev. Lett.* **114** (11), 118301.

MAO, M., SHERWOOD, J. D. & GHOSAL, S. 2014 Electro-osmotic flow through a nanopore. *J. Fluid Mech.* **749**, 167–183.

MARCUS, Y. 2007 Gibbs energies of transfer of anions from water to mixed aqueous organic solvents. *Chem. Rev.* **107** (9), 3880–3897.

MICHLER, D., SHAHIDZADEH, N., WESTBROEK, M., VAN ROIJ, R. & BONN, D. 2015 Are antagonistic salts surfactants? *Langmuir* **31** (3), 906–911.

NELLEN, U., DIETRICH, J., HELDEN, L., CHODANKAR, S., NYGÅRD, K., VAN DER VEEN, J. F. & BECHINGER, C. 2011 Salt-induced changes of colloidal interactions in critical mixtures. *Soft Matt.* **7**, 5360–5364.

OKAMOTO, R. & ONUKI, A. 2011 Charged colloids in an aqueous mixture with a salt. *Phys. Rev.* E **84**, 051401.

ONUKI, A. & KITAMURA, H. 2004 Solvation effects in near-critical binary mixtures. *J. Chem. Phys.* **121** (7), 3143–3151.

ONUKI, A., YABUNAKA, S., ARAKI, T. & OKAMOTO, R. 2016 Structure formation due to antagonistic salts. *Curr. Opin. Colloid Interface Sci.* **22**, 59–64.

POUSANEH, F. & CIACH, A. 2011 The origin of the attraction between like charged hydrophobic and hydrophilic walls confining a near-critical binary aqueous mixture with ions. *J. Phys.: Condens. Matter* **23** (41), 412101.

POUSANEH, F. & CIACH, A. 2014 The effect of antagonistic salt on a confined near-critical mixture. *Soft Matt.* **10** (41), 8188–8201.

RANKIN, D. J. & HUANG, D. M. 2016 The effect of hydrodynamic slip on membrane-based salinity-gradient-driven energy harvesting. *Langmuir* **32** (14), 3420–3432.

SAMIN, S., HOD, M., MELAMED, E., GOTTLIEB, M. & TSORI, Y. 2014 Experimental demonstration of the stabilization of colloids by addition of salt. *Phys. Rev. Appl.* **2** (2), 024008.

SAMIN, S. & VAN ROIJ, R. 2017 Interplay between adsorption and hydrodynamics in nanochannels: towards tunable membranes. *Phys. Rev. Lett.* **118** (1), 014502.

SAMIN, S. & TSORI, Y. 2011 Attraction between like-charge surfaces in polar mixtures. *Europhys. Lett.* **95** (3), 36002.

SAMIN, S. & TSORI, Y. 2012 The interaction between colloids in polar mixtures above t_c. *J. Chem. Phys.* **136** (15), 154908.

SAMIN, S. & TSORI, Y. 2013 Stabilization of charged and neutral colloids in salty mixtures. *J. Chem. Phys.* **139** (24), 244905.

SAMIN, S. & TSORI, Y. 2016 Reversible pore gating in aqueous mixtures via external potential. *Colloid Interface Sci. Commun.* **12**, 9–12.

SAZONOV, V. P., SHAW, D. G., SKRZECZ, A., LISOV, N. I. & SAZONOV, N. V. 2007 IUPAC-NIST solubility data series. 83. Acetonitrile: ternary and quaternary systems. *J. Phys. Chem. Ref. Data* **36** (3), 733–1131.

VON SMOLUCHOWSKI, M. 1903 Contribution à la théorie de l'endosmose électrique et de quelques phénomnès corrélatifs. *Bull. Intl Acad. Sci. Cracovie* **8**, 182.

SQUIRES, T. M. & QUAKE, S. R. 2005 Microfluidics: fluid physics at the nanoliter scale. *Rev. Mod. Phys.* **77** (3), 977–1026.

STONE, H. A., STROOCK, A. D. & AJDARI, A. 2004 Engineering flows in small devices. *Annu. Rev. Fluid Mech.* **36** (1), 381–411.

TSORI, Y. & LEIBLER, L. 2007 Phase-separation in ion-containing mixtures in electric fields. *Proc. Natl Acad. Sci. USA* **104** (18), 7348–7350.

VALKÓ, I. E., SIRÉN, H. & RIEKKOLA, M.-L. 1999 Characteristics of electroosmotic flow in capillary electrophoresis in water and in organic solvents without added ionic species. *J. Microcolumn. Separations* **11** (3), 199–208.

WOHLFARTH, C. 2009 Viscosity of pure organic liquids and binary liquid mixtures. In *Landolt-Börnstein: Numerical Data and Functional Relationships in Science and Technology*, vol. IV/25. Springer.

ZWANIKKEN, J. & VAN ROIJ, R. 2007 Charged colloidal particles and small mobile ions near the oil–water interface: destruction of colloidal double layer and ionic charge separation. *Phys. Rev. Lett.* **99**, 178301.